Ultrahigh-energy diffuse gamma-ray emission from cosmic-ray interactions with the medium surrounding acceleration sources

Pei-pei Zhang[1,2,3,4] Bing-qiang Qiao[4,*] Qiang Yuan,[1,2] Shu-wang Cui,[3] and Yi-qing Guo[4,5,†]

[1]*Key Laboratory of Dark Matter and Space Astronomy, Purple Mountain Observatory,*
Chinese Academy of Sciences, Nanjing 210023, China
[2]*School of Astronomy and Space Science, University of Science and Technology of China,*
Hefei 230026, Anhui, China
[3]*Hebei Normal University, Shijiazhuang 050024, Hebei, China*
[4]*Key Laboratory of Particle Astrophysics, Institute of High Energy Physics, Chinese Academy of Sciences,*
Beijing 100049, China
[5]*University of Chinese Academy of Sciences, Beijing 100049, China*

The diffuse γ-ray spectrum at sub-PeV energy region has been measured for the first time by the Tibet-ASγ experiment. It will shed new light on the understanding of the origin and propagation of Galactic cosmic rays at very high energies. It has been pointed out that the traditional cosmic ray propagation model based on low energy measurements undershoot the new data, and modifications of the model with new ingredients or alternative propagation framework is required. In this work, we propose that the hadronic interactions between freshly accelerated cosmic rays and the medium surrounding the sources, which was neglected in the traditional model, can naturally account for the Tibet-ASγ diffuse emission. We show that this scenario gives a consistent description of other secondary species such as the positron spectrum, the boron-to-carbon ratio, and the antiproton-to-proton ratio. As a result, the electron spectrum above 10 TeV will have a hardening due to this secondary component, which may be tested by future measurements.

I. INTRODUCTION

The Galactic diffuse γ-ray emission (DGE) is expected to be produced by interactions between cosmic rays (CRs) and the interstellar medium (ISM) as well as the interstellar radiation field (ISRF), during the propagation of CRs in the Milky Way. The DGE includes mainly three components: the decay of π^0 from inelastic hadronic interactions between CR nuclei and the ISM, the bremsstrahlung of CR electrons and positrons (CREs) in the ISM, and the inverse Compton scattering (ICS) component of CREs scattering off the ISRF [1]. This model can consistently describe most of the DGE data below 100 GeV and the locally observed results of CRs [2–4], with only slight excesses in the inner Galactic plane which was suggested to be due to unresolved sources or spectral variations of CRs throughout the Milky Way [4]. Measurements of DGE at higher energies are thus very important to further test the model.

The ground based experiments Milagro and ARGO-YBJ measured the DGE above TeV energies, for a few selected sky regions along the Galactic plane [5–7]. Particularly, in the Cygnus region, the Milagro observation identified an excess [5] compared with the CR propagation model tuned to account for the low-energy DGE [2]. Some fresh sources in such a region may explain the excess [8,9]. Very recently, the DGE in the Galactic plane above 100 TeV energies was for the first time measured by the Tibet-ASγ experiment [10], which has attracted wide attention for possible physical discussion [11–23]. The Tibet-ASγ fluxes are higher than the prediction of the conventional CR propagation model, and additional components or modification of the conventional propagation framework may be needed [10,14,15].

However, in the traditional DGE modeling the secondary particle production (including γ rays) due to interactions between newly accelerated CRs and the gas surrounding the sources is usually omitted. This component may not be small [24], and is expected to be more and more important at high energies since the CR spectra around the sources are harder than those diffusing out in the Milky Way. The possible confinement of CRs around the sources may further enhance this component of secondary particles. In this work, we investigate this scenario in light of the ultrahigh-energy (UHE) diffuse emission measured by Tibet-ASγ. The consequence of such interactions for other types of secondary particles, such as the B/C ratio, the positron and antiproton fluxes will also be investigated.

*[*]qiaobq@ihep.ac.cn
[†]guoyq@ihep.ac.cn

We confront this model with the up-to-date measurements of γ rays and CRs, and find a consistent description of these new data.

II. MODEL DESCRIPTION

A. Propagation of CRs

It has been recognized in recent years that the propagation of CRs in the Milky Way should depend on the spatial locations, as inferred by the HAWC and LHAASO observations of extended γ-ray halos around pulsars [25,26] and the spatial variations of the CR intensities and spectral indices from Fermi-LAT observations [27,28]. The spatially-dependent propagation (SDP) model was also proposed to explain the observed hardenings of CRs [29–35], and also the large-scale anisotropies with the help of a nearby source [36–38].

In the SDP model, the diffusive halo is divided into two parts, the inner halo (disk) and the outer halo. In the inner halo, the diffusion coefficient is much smaller than that in the outer halo, as indicated by the pulsar halo observations. To enable a smooth variation of the diffusion coefficient D_{xx}, we parametrize it as

$$D_{xx}(r, z, \mathcal{R}) = D_0 F(r, z) \beta^\eta \left(\frac{\mathcal{R}}{\mathcal{R}_0}\right)^{\delta_0 F(r,z)}, \quad (1)$$

where r and z are cylindrical coordinate, $\mathcal{R}$ is the particle's rigidity, β is the particle's velocity in unit of light speed, D_0 and δ_0 are constants representing the diffusion coefficient and its high-energy rigidity dependence in the outer halo, η is a phenomenological constant in order to fit the low-energy data. The spatial dependence function $F(r, z)$ is given as [35],

$$F(r, z) = \begin{cases} g(r, z) + [1 - g(r, z)] \left(\frac{z}{\xi z_h}\right)^n, & |z| \le \xi z_h \\ 1, & |z| > \xi z_h \end{cases}, \quad (2)$$

in which $g(r, z) = N_m / [1 + f(r, z)]$, and $f(r, z)$ is the source density distribution (see below Sec. II B), z_h is the half-thickness of the propagation cylinder, and ξz_h is the half-thickness of the inner halo. The factor $\left(\frac{z}{\xi z_h}\right)^n$ describes the smoothness of the parameters at the transition between the two halos. Note that the spatial dependence of the diffusion coefficient is phenomenologically assumed. Physically it may be related with the magnetic field distribution, or possibly the turbulence driven by CRs [39]. The model parameters used in this work are listed in Table I. We adopt

the diffusion reacceleration model in this work, with the reacceleration being described by a diffusion in the momentum space. The momentum diffusion coefficient, D_{pp}, correlates with D_{xx} via $D_{pp}D_{xx} = \frac{4p^2 v_A^2}{3\delta(4-\delta^2)(4-\delta)}$, where v_A is the Alfvén velocity, p is the momentum, and δ is the rigidity dependence slope of the spatial diffusion coefficient [40]. The numerical package DRAGON is used to solve the propagation equation of CRs [41]. For energies smaller than tens of GeV, the fluxes of CRs are suppressed by the solar modulation effect. We use the force-field approximation [42] to account for the solar modulation.

B. Background source distribution

Supernova remnants (SNRs) are considered to be the most plausible candidates for the acceleration of CRs. The spatial distribution of SNRs are approximated as an axisymmetric form parametrized as

$$f(r, z) = \left(\frac{r}{r_\odot}\right)^\alpha \exp\left[-\frac{\beta(r - r_\odot)}{r_\odot}\right] \exp\left(-\frac{|z|}{z_s}\right), \quad (3)$$

where $r_\odot \equiv 8.5$ kpc represents the distance from the Galactic center to the solar system. Parameters α and β are taken to be 1.69 and 3.33 [43]. The density of the SNR distribution decreases exponentially along the vertical height from the Galactic plane, with $z_s = 200$ pc.

The injection spectrum of nuclei and primary electrons are assumed to be an exponentially cutoff broken power-law function of particle rigidity $\mathcal{R}$

$$q(\mathcal{R}) = q_0 \begin{cases} \left(\frac{\mathcal{R}}{\mathcal{R}_{br}}\right)^{\nu_1}, & \mathcal{R} \le \mathcal{R}_{br} \\ \left(\frac{\mathcal{R}}{\mathcal{R}_{br}}\right)^{\nu_2} \exp\left[-\frac{\mathcal{R}}{\mathcal{R}_c}\right], & \mathcal{R} > \mathcal{R}_{br} \end{cases}, \quad (4)$$

where q_0 is the normalization factor, $\nu_{1,2}$ are the spectral incides, $\mathcal{R}_{br}$ is break rigidity, $\mathcal{R}_c$ is the cutoff rigidity. The spectral break is employed to fit the low-energy spectra of CRs, which is not the focus of the current work.

C. Local pulsar and local SNR

At TeV energies, CREs originate from sources within ~ 1 kpc around the solar system [44]. In this small region, the hypothesis of continuous distribution may not be valid any more. Studies show that the discrete effect of nearby CR sources could induce large fluctuations, especially at high energies [45–47]. The contribution of nearby sources to CREs has been studied in the past works

TABLE I. Propagation parameters of the SDP model.

D_0 [10^{28} cm^2/s]	δ	N_m	ξ	n	η	$\mathcal{R}_0$ [GV]	v_A [km/s]	z_h [kpc]
4.9	0.55	0.57	0.1	4	0.05	2	6	5

(see e.g., [48–51]). In this work, we assume a nearby pulsar to account for the positron excess above ~20 GeV. The propagation of CREs injected instantaneously from a point source is described by a time-dependent propagation equation [52]. The injection rate as a function of time and rigidity is assumed to be

$$Q^{\mathrm{psr}}(\mathcal{R}, t) = Q_0^{\mathrm{psr}}(t) \left(\frac{\mathcal{R}}{\mathcal{R}_0} \right)^{-\gamma} \exp \left[-\frac{\mathcal{R}}{\mathcal{R}_c^{e_\pm}} \right], \quad (5)$$

where $\mathcal{R}_c^{e_\pm}$ is the cutoff rigidity of its accelerated CREs. A continuous injection process of electron and positron pairs with injection rate proportional to the spindown power of the pulsar is assumed, i.e.,

$$Q_0^{\mathrm{psr}}(t) \propto \frac{q_0^{\mathrm{psr}}}{\tau_0 (1 + t/\tau_0)^2}, \quad (6)$$

where τ_0 is a characteristic time scale of the decay of the spindown [53,54].

The progenitor of this pulsar produces an SNR, which may accelerate primary nuclei and electrons during its early evolution stage. This local source contribution of primary electrons may be necessary, given the different spectral behaviors of positrons and electrons [55]. The injection process of the SNR is approximated as burstlike. The source injection rate is assumed to be the same as Eq. (5) but with

$$Q_0^{\mathrm{snr}}(t) = q_0^{\mathrm{snr}} \delta(t - t_0), \quad (7)$$

where t_0 is the time of the supernova explosion. The propagated spectrum from the local pulsar and SNR is thus a convolution of the Green's function and the time-dependent injection rate $Q_0(t)$ [52]

$$\varphi(\boldsymbol{r}, \mathcal{R}, t) = \int_{t_i}^{t} G(\boldsymbol{r} - \boldsymbol{r}', t - t', \mathcal{R}) Q_0(t') dt'. \quad (8)$$

The normalization is determined through fitting Galactic cosmic rays energy spectra, which results in a total energy of $\sim 2.3 \times 10^{50}$ erg for protons and $\sim 1.4 \times 10^{50}$ erg for helium. If 10% of kinetic energy is used to accelerate CRs, the total energy of supernova explosion is estimated to $\sim 3.7 \times 10^{51}$ erg. Note that the local source introduced here is to account for the energy spectra of CRs, and is independent of the excess of the UHE diffuse γ rays.

D. Secondary particles from interactions of freshly accelerated CRs

The freshly accelerated CRs at sources could also interact with the surrounding gas before they escape from the source regions and enter the diffusive halo. Secondary electrons, positrons, antiprotons, and γ rays could be produced, whose yields can be calculated as

$$Q_{\mathrm{sec},j} = \sum_{i=\mathrm{p,He}} \int_{E_{\mathrm{th}}}^{+\infty} dE_i\, v \left\{ n_{\mathrm{H}} \frac{d\sigma_{i+\mathrm{H} \to j}}{dE_j} \right.$$
$$\left. + n_{\mathrm{He}} \frac{d\sigma_{i+\mathrm{He} \to j}}{dE_j} \right\} Q_i(E_i), \quad (9)$$

where $n_{\mathrm{H,He}}$ is the number density of hydrogen and helium, $d\sigma_{i+\mathrm{H} \to j}/dE_j$ is the differential cross section of the production of secondary particle j from primary particle i. The yields of secondary nuclei (such as boron) are simply

$$Q_{\mathrm{B},j} = \sum_{i=\mathrm{C,N,O}} (n_{\mathrm{H}} \sigma_{i+\mathrm{H} \to j} + n_{\mathrm{He}} \sigma_{i+\mathrm{He} \to j}) v Q_i(E). \quad (10)$$

Secondary charge particles also propagate in the Galaxy, which are also calculated with the DRAGON package.

III. RESULTS

A. Spectra of CR nuclei

The left panel of Fig. 1 shows the proton spectrum expected from the model, compared with the measurements [56–59]. The model parameters for different source components are given in Table II. The hardening of the proton spectrum around several hundred GeV can be attributed to the summation of the background contribution and the local SNR contribution, and the softening around 14 TeV is mainly due to the spectral cutoff of the local SNR. Similar spectral features are expected to be present for all species, as revealed recently by the DAMPE helium spectral measurement [60]. In the right panel of Fig. 1 we show the total spectrum of high-abundance nuclei, compared with the data [59]. For the parameters we adopt, the knee of the all-particle spectrum is mainly due to the spectral cutoff of protons and helium nuclei from the background SNRs.

B. Diffuse γ rays

The DGE is produced through three major processes: decay of π^0 produced in pp-collisions, ICS and bremsstrahlung of CREs. At high energies, the π^0 decay component dominates the DGE. Therefore we only consider the π^0 decay component in the following calculation. Comparisons between the model calculation and the measurements by ARGO-YBJ [7] and Tibet-ASγ [10] are given in Fig. 2, for two sky regions, $25° < l < 100°$, $|b| < 5°$ and $50° < l < 200°$, $|b| < 5°$, respectively. The DGE fluxes from the background sources are lower by a factor of several than the data, as also shown in [15]. The inclusion of the secondary production from freshly accelerated CRs interacting with the surrounding gas, which has a harder spectrum than the CRs diffusing out, can reproduce the data well. We can also estimate the interaction time of the source component, which is about 5×10^5 years for the Galactic gas density distribution as adopted in
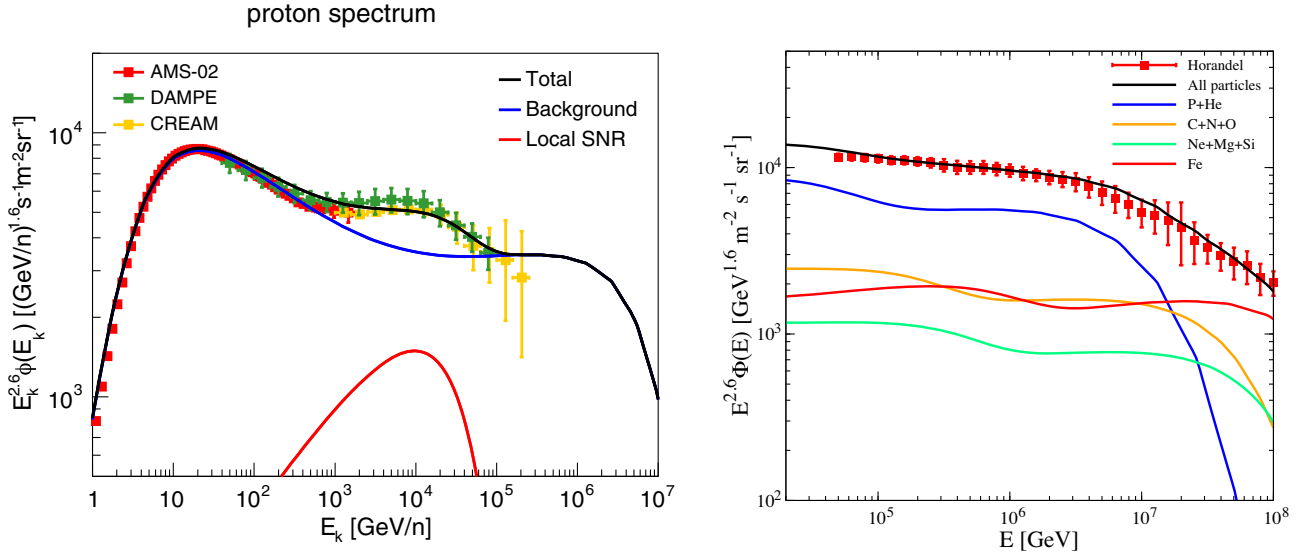
FIG. 1.   The spectra of protons (left) and all particles (right). The measurements of proton spectra are from AMS-02 [56], CREAM [57], and DAMPE [58]. The all-particle spectrum is taken from the normalized result of [59].
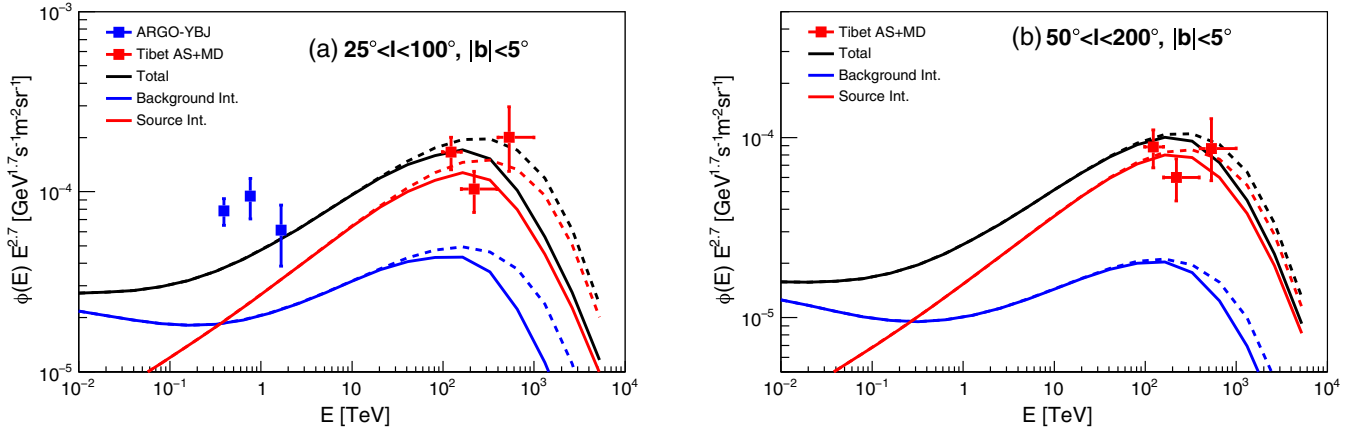

FIG. 2.   Diffuse γ-ray spectra from the model calculation, compared with the measurements by ARGO-YBJ [7] and Tibet ASγ [10]. The dashed and solid lines are the model predictions without and with the absorption in the Milky Way ISRF.

DRAGON. It may be even shorter if some of the sources were located in denser molecular medium. This time reflects the confinement time of CRs in the vicinity of the sources. Note that at very high energies ($E \gtrsim 100$ TeV), the absorption of γ rays due to pair production with ISRF becomes important [61], which leads to a reduction of the DGE spectrum, as shown by the solid line.

C. Ratios of B/C and $\bar{p}/p$

The same process to produce secondary γ rays will generate simultaneously secondary boron nuclei and antiprotons. The results of the B/C and the $\bar{p}/p$ ratios are shown in Fig. 3. Good consistency between the model and the data can be seen. We note that the contribution of the "fresh" component exceeds the background component when $E \gtrsim 100$ GeV for γ rays and antiprotons, but it happens

at much higher energies for B/C. This is due to the fact that energies of secondary particles from inelastic pp interactions are much lower than those of parent protons. However, for the nuclear fragmentation the kinetic energy per nucleon keeps almost unchanged. Note that for kinetic energies higher than ~ 100 GeV, the measured $\bar{p}/p$ is slightly higher than the model prediction. Further refinement of the model parameters or additional source of antiprotons such as the dark matter annihilation [62,63] may improve fitting to the data. This may also not be an issue due to the relatively large uncertainties of the measurements.

D. Spectra of electrons and positrons

Finally we discuss the results of positrons and electrons. There are three components of CR positrons, the secondary contributions from CRs interacting when
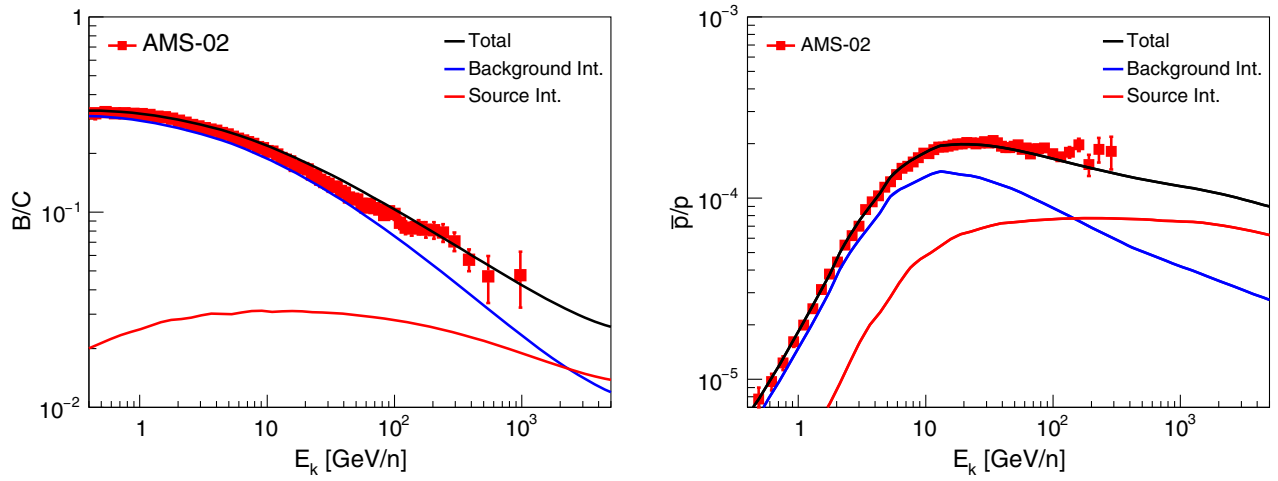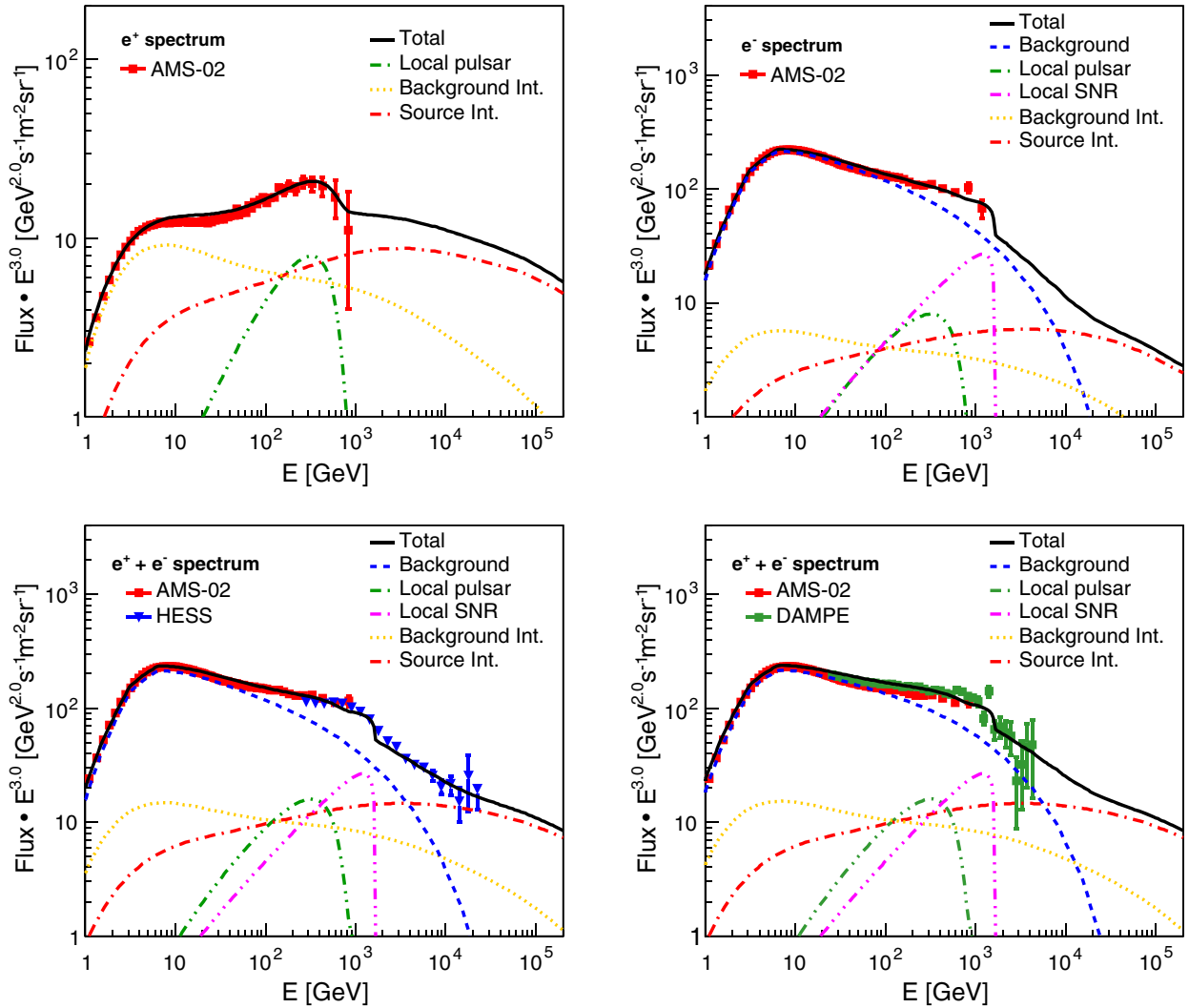
FIG. 3.   The secondary-to-primary ratios of B/C (left) and $\bar{p}/p$ (right). The data are from AMS-02 [64,65].

FIG. 4.   The spectra of positrons and electrons (top) and total spectra of positrons plus electrons (bottom). The measurements are from AMS-02 [68,69], H.E.S.S. [66], and DAMPE [67].

TABLE II. Injection parameters of different source components.

Background	Q_0 [m^{-2} sr^{-1} s^{-1} GeV^{-1}][†]	ν_1	$\mathcal{R}_{\rm br}$ [GV]	ν_2	$\mathcal{R}_{\rm c}$ [GV]	
e^- for HESS fitting	2.70×10^{-1}	1.14	4.5	2.77	1×10^4	
e^- for DAMPE fitting	2.60×10^{-1}	1.14	4.5	2.70	1.1×10^4	
P	4.49×10^{-2}	2.20	7.2	2.38	7×10^6	
He	3.74×10^{-3}	2.20	7.2	2.32	7×10^6	
C	1.14×10^{-4}	2.20	7.2	2.32	7×10^6	
N	9.18×10^{-6}	2.20	7.2	2.35	7×10^6	
O	1.27×10^{-4}	2.20	7.2	2.37	7×10^6	
Ne	1.62×10^{-5}	2.20	7.2	2.30	7×10^6	
Mg	3.45×10^{-6}	2.20	7.2	2.36	7×10^6	
Si	1.91×10^{-5}	2.20	7.2	2.39	7×10^6	
Fe	1.82×10^{-5}	2.20	7.2	2.31	7×10^6	
Local pulsar	$r_{\rm psr}$ [kpc]	$t_{\rm inj}$ [yrs]	$q_0^{\rm psr}$ [GeV^{-1}]	γ	$\mathcal{R}_{\rm c}^{\rm e\pm}$ [GV]	τ_0 [yrs]
	0.33	3.3×10^5	2.7×10^{49}	1.90	800	10^4
Local SNR	$r_{\rm snr}$ [kpc]	$t_{\rm inj}$ [yrs]	$q_0^{\rm snr}$ [GeV^{-1}]	γ	$\mathcal{R}_{\rm c}$ [GV]	
e^-	0.33	3.3×10^5	5.0×10^{49}	2.10	2.8×10^4	
P	0.33	3.3×10^5	2.4×10^{52}	2.10	2.8×10^4	
He	0.33	3.3×10^5	1.5×10^{52}	2.08	2.8×10^4	
C	0.33	3.3×10^5	7.2×10^{50}	2.13	2.8×10^4	
N	0.33	3.3×10^5	1.1×10^{50}	2.13	2.8×10^4	
O	0.33	3.3×10^5	7.5×10^{50}	2.13	2.8×10^4	
Ne	0.33	3.3×10^5	1.1×10^{50}	2.13	2.8×10^4	
Mg	0.33	3.3×10^5	1.0×10^{50}	2.13	2.8×10^4	
Si	0.33	3.3×10^5	1.0×10^{50}	2.13	2.8×10^4	
Fe	0.33	3.3×10^5	1.8×10^{50}	2.13	2.8×10^4	

propagating in the Milky Way and around the acceleration sources, and the primary contribution from the local pulsar. For CR electrons, besides the same components as positrons, there are additional primary components from both the background sources and the local SNR. The results are given in Fig. 4. Model parameters of electrons are also given in Table II. For the total CRE spectra, we give two groups of parameters according to the fittings to the H.E.S.S. [66] and DAMPE [67] data, which differ slightly. A clear feature of the model prediction is that for energies above TeV, the fresh CR interactions dominate the positron and electron spectra, resulting in hardenings of their spectra. Such a property may be tested by further precise measurements of the positron and electron spectra.

IV. CONCLUSION

The DGE at ultra-high energies is believed to be produced through the interaction of CRs with the ISM, and is thus a good tracer to study the propagation of galactic CRs. The ever first measurements of DGE above 100 TeV energies by Tibet-ASγ recently shows a significant excess compared with the conventional CR propagation and interaction model prediction. We find that possible hadronic interactions of CRs with ambient gas surrounding the acceleration sources can account for the ultra-high energy DGE by Tibet-ASγ. The harder spectrum of CRs in the vicinity of the sources can naturally explain the high-energy part of the DGE, while keeps the low-energy part unaffected. The secondary interactions around the sources generate simultaneously positrons and electrons, antiprotons, and boron nuclei. With proper model parameters, we find that all these CR measurements can be well reproduced. This model predicts hardenings of the spectra of both positrons and electrons above TeV energies, and can be tested with future measurements.

[1] A. W. Strong, I. V. Moskalenko, and V. S. Ptuskin, Cosmic-ray propagation and interactions in the galaxy, Annu. Rev. Nucl. Part. Sci. **57,** 285 (2007).

[2] A. W. Strong, I. V. Moskalenko, and O. Reimer, Diffuse galactic continuum gamma rays: A model compatible with EGRET data and cosmic-ray measurements, Astrophys. J. **613,** 962 (2004).

[3] J. Zhang, Q. Yuan, and X.-J. Bi, Galactic diffuse gamma rays—recalculation based on new measurements of the cosmic electron spectrum, Astrophys. J. **720,** 9 (2010).

[4] M. Ackermann, M. Ajello, W. B. Atwood et al., Fermi-LAT observations of the diffuse γ-ray emission: Implications for cosmic rays and the interstellar medium, Astrophys. J. **750,** 3 (2012).

[5] A. A. Abdo, B. Allen, D. Berley et al., Discovery of TeV gamma-ray emission from the Cygnus region of the galaxy, Astrophys. J. **658,** L33 (2007).

[6] A. A. Abdo, B. Allen, T. Aune et al., A measurement of the spatial distribution of diffuse TeV gamma-ray emission from the galactic plane with Milagro, Astrophys. J. **688,** 1078 (2008).

[7] B. Bartoli, P. Bernardini, X. J. Bi et al., Study of the diffuse gamma-ray emission from the galactic plane with ARGO-YBJ, Astrophys. J. **806,** 20 (2015).

[8] X. J. Bi, T. L. Chen, Y. Wang, and Q. Yuan, The diffuse GeV-TeV γ-ray emission of the Cygnus region, Astrophys. J. **695,** 883 (2009).

[9] Y.-Q. Guo, H.-B. Hu, and Z. Tian, On the contribution of a hard galactic plane component to the excesses of secondary particles, Chin. Phys. C **40,** 115001 (2016).

[10] M. Amenomori, Y. W. Bao, X. J. Bi et al., First Detection of Sub-PeV Diffuse Gamma Rays from the Galactic Disk: Evidence for Ubiquitous Galactic Cosmic Rays Beyond PeV Energies, Phys. Rev. Lett. **126,** 141101 (2021).

[11] S. S. Kimura, T. Sudoh, K. Kashiyama, and N. Kawanaka, Magnetically arrested disks in quiescent black-hole binaries: Formation scenario, observable signatures, and potential PeVatrons, Astrophys. J. **915,** 31 (2021).

[12] T. Dzhatdoev, Implications of the detection of sub-PeV diffuse γ rays from the Galactic disk apart from discrete sources, arXiv:2104.02838.

[13] K. Fang and K. Murase, Multi-messenger implications of sub-PeV diffuse galactic gamma-ray emission, Astrophys. J. **919,** 93 (2021).

[14] R.-Y. Liu and X.-Y. Wang, Origin of galactic sub-PeV diffuse gamma-ray emission: Constraints from high-energy neutrino observations, Astrophys. J. Lett. **914,** L7 (2021).

[15] B.-Q. Qiao, W. Liu, M.-J. Zhao, X.-J. Bi, and Y.-Q. Guo, Galactic cosmic ray propagation: Sub-PeV diffuse gamma-ray and neutrino emission, arXiv:2104.03729.

[16] P. Huentemeyer, Signs of PeVatrons in gamma-ray haze, Phys. Online J. **14,** 41 (2021), https://ui.adsabs.harvard.edu/abs/2021PhyOJ..14...41H.

[17] A. Esmaili and P. D. Serpico, First implications of Tibet ASγ data for heavy dark matter, Phys. Rev. D **104,** L021301 (2021).

[18] S. Koldobskiy, A. Neronov, and D. Semikoz, Pion decay model of TIBET-ASγPeV gamma-ray signal, Phys. Rev. D **104,** 043010 (2021).

[19] M. Bouyahiaoui, M. Kachelriess, and D. V. Semikoz, A hot spot in the neutrino flux created by cosmic rays from the Cygnus Loop, Proc. Sci., ICRC2021 (**2021**) 999 [arXiv:2105.13378].

[20] D. D. Dzhappuev, Yu. Z. Afashokov, I. M. Dzaparova et al., Observation of photons above 300 TeV associated with a high-energy neutrino from the Cygnus Cocoon region, Astrophys. J. Lett. **916,** L22 (2021).

[21] C. Li and B.-Q. Ma, Light speed variation in a string theory model for space-time foam, Phys. Lett. B **819,** 136443 (2021).

[22] L. Tibaldo, D. Gaggero, and P. Martin, Gamma rays as probes of cosmic-ray propagation and interactions in galaxies, Universe **7,** 141 (2021).

[23] T. N. Maity, A. K. Saha, A. Dubey, and R. Laha, A search for dark matter using sub-PeV γ-rays observed by Tibet ASγ, arXiv:2105.05680.

[24] R. Yang and F. Aharonian, Interpretation of the excess of antiparticles within a modified paradigm of galactic cosmic rays, Phys. Rev. D **100,** 063020 (2019).

[25] A. U. Abeysekara, A. Albert, R. Alfaro et al., Extended gamma-ray sources around pulsars constrain the origin of the positron flux at Earth, Science **358,** 911 (2017).

[26] F. Aharonian, Q. An, L. X. Axikegu, Bai et al., Extended Very-High-Energy Gamma-Ray Emission Surrounding PSR J0622 + 3749 Observed by LHAASO-KM2A, Phys. Rev. Lett. **126,** 241103 (2021).

[27] R. Yang, F. Aharonian, and C. Evoli, Radial distribution of the diffuse γ -ray emissivity in the Galactic disk, Phys. Rev. D **93,** 123007 (2016).

[28] F. Acero, M. Ackermann, M. Ajello et al., Development of the model of galactic interstellar emission for standard point-source analysis of Fermi large area telescope data, Astrophys. J. Suppl. Ser. **223,** 26 (2016).

[29] N. Tomassetti, Origin of the cosmic-ray spectral hardening, Astrophys. J. Lett. **752,** L13 (2012).

[30] N. Tomassetti, Cosmic-ray protons, nuclei, electrons, and antiparticles under a two-halo scenario of diffusive propagation, Phys. Rev. D **92,** 081301 (2015).

[31] J. Feng, N. Tomassetti, and A. Oliva, Bayesian analysis of spatial-dependent cosmic-ray propagation: Astrophysical background of antiprotons and positrons, Phys. Rev. D **94,** 123007 (2016).

[32] Y.-Q. Guo, Z. Tian, and C. Jin, Spatial-dependent propagation of cosmic rays results in the spectrum of proton, ratios of P/P, and B/C, and anisotropy of nuclei, Astrophys. J. **819,** 54 (2016).

[33] W. Liu, Y.-h. Yao, and Y.-Q. Guo, Revisiting the spatially dependent propagation model with the latest observations of cosmic-ray nuclei, Astrophys. J. **869,** 176 (2018).

[34] Y.-Q. Guo and Q. Yuan, Understanding the spectral hardenings and radial distribution of Galactic cosmic rays and Fermi diffuse γ rays with spatially-dependent propagation, Phys. Rev. D **97,** 063008 (2018).

[35] Z. Tian, W. Liu, B. Yang, X.-D. Fu, H.-B. Xu, Y.-H. Yao, and Y.-Q. Guo, Electron and positron spectra in three-dimensional spatial-dependent propagation model, Chin. Phys. C **44,** 085102 (2020).

[36] W. Liu, Y.-Q. Guo, and Q. Yuan, Indication of nearby source signatures of cosmic rays from energy spectra and anisotropies, J. Cosmol. Astropart. Phys. 10 (2019) 010.

[37] B.-Q. Qiao, W. Liu, Y.-Q. Guo, and Q. Yuan, Anisotropies of different mass compositions of cosmic rays, J. Cosmol. Astropart. Phys. 12 (2019) 007.

[38] Q. Yuan, B.-Q. Qiao, Y.-Q. Guo, Y.-Z. Fan, and X.-J. Bi, Nearby source interpretation of differences among light and medium composition spectra in cosmic rays, Front. Phys. **16,** 24501 (2021).

[39] P. Blasi, E. Amato, and P. D. Serpico, Spectral Breaks as a Signature of Cosmic Ray Induced Turbulence in the Galaxy, Phys. Rev. Lett. **109,** 061101 (2012).

[40] E. S. Seo and V. S. Ptuskin, Stochastic reacceleration of cosmic rays in the interstellar medium, Astrophys. J. **431,** 705 (1994).

[41] C. Evoli, D. Gaggero, A. Vittino, G. Di Bernardo, M. Di Mauro, A. Ligorini, P. Ullio, and D. Grasso, Cosmic-ray propagation with DRAGON2: I. Numerical solver and astrophysical ingredients, J. Cosmol. Astropart. Phys. 2 (2017) 015.

[42] L. J. Gleeson and W. I. Axford, Solar modulation of galactic cosmic rays, Astrophys. J. **154,** 1011 (1968).

[43] G. Case and D. Bhattacharya, Revisiting the galactic supernova remnant distribution, Astron. Astrophys. Suppl. Ser. **120,** 437 (1996), https://ui.adsabs.harvard.edu/abs/1996A&AS..120C.437C.

[44] Q. Yuan and L. Feng, Dark matter particle explorer observations of high-energy cosmic ray electrons plus positrons and their physical implications, Sci. China Phys. Mech. Astron. **61,** 101002 (2018).

[45] P. Mertsch, Cosmic ray electrons and positrons from discrete stochastic sources, J. Cosmol. Astropart. Phys. 02 (2011) 031.

[46] G. Bernard, T. Delahaye, P. Salati, and R. Taillet, Variance of the Galactic nuclei cosmic ray flux, Astron. Astrophys. **544,** A92 (2012).

[47] K. Fang, B.-B. Wang, X.-J. Bi, S.-J. Lin, and P.-F. Yin, Perspective on the cosmic-ray electron spectrum above TeV, Astrophys. J. **836,** 172 (2017).

[48] P. D. Serpico, Astrophysical models for the origin of the positron "excess", Astropart. Phys. **39,** 2 (2012).

[49] M. Di Mauro, F. Donato, N. Fornengo, R. Lineros, and A. Vittino, Interpretation of AMS-02 electrons and positrons data, J. Cosmol. Astropart. Phys. 04 (2014) 006.

[50] W. Liu, X.-J. Bi, S.-J. Lin, B.-B. Wang, and P.-F. Yin, Excesses of cosmic ray spectra from a single nearby source, Phys. Rev. D **96,** 023006 (2017).

[51] K. Fang, X.-J. Bi, and P.-F. Yin, Explanation of the Knee-like feature in the DAMPE cosmic $e^- + e^+$ energy spectrum, Astrophys. J. **854,** 57 (2018).

[52] A. M. Atoyan, F. A. Aharonian, and H. J. Völk, Electrons and positrons in the galactic cosmic rays, Phys. Rev. D **52,** 3265 (1995).

[53] N. Kawanaka, K. Ioka, and M. M. Nojiri, Is cosmic ray electron excess from pulsars spiky or smooth?: Continuous and multiple electron/positron injections, Astrophys. J. **710,** 958 (2010).

[54] P.-F. Yin, Z.-H. Yu, Q. Yuan, and X.-J. Bi, Pulsar interpretation for the AMS-02 result, Phys. Rev. D **88,** 023001 (2013).

[55] P.-p. Zhang, B.-q. Qiao, W. Liu, S.-w. Cui, Q. Yuan, and Y.-q. Guo, Possible bump structure of cosmic ray electrons unveiled by AMS-02 data and its common origin along with the nuclei and positron, J. Cosmol. Astropart. Phys. 5 (2021) 012.

[56] M. Aguilar, D. Aisa, B. Alpat et al., Precision Measurement of the Proton Flux in Primary Cosmic Rays from Rigidity 1 GV to 1.8 TV with the Alpha Magnetic Spectrometer on the International Space Station, Phys. Rev. Lett. **114,** 171103 (2015).

[57] Y. S. Yoon, T. Anderson, A. Barrau et al., Proton and helium spectra from the CREAM-III flight, Astrophys. J. **839,** 5 (2017).

[58] Q. An, R. Asfandiyarov, P. Azzarello et al., Measurement of the cosmic ray proton spectrum from 40 GeV to 100 TeV with the DAMPE satellite, Sci. Adv. **5,** eaax3793 (2019).

[59] J. R. Hörandel, On the knee in the energy spectrum of cosmic rays, Astropart. Phys. **19,** 193 (2003).

[60] F. Alemanno, Q. An, P. Azzarello et al., Measurement of the Cosmic Ray Helium Energy Spectrum from 70 GeV to 80 TeV with the DAMPE Space Mission, Phys. Rev. Lett. **126,** 201102 (2021).

[61] J.-L. Zhang, X.-J. Bi, and H.-B. Hu, Very high energy γ ray absorption by the galactic interstellar radiation field, Astron. Astrophys. **449,** 641 (2006).

[62] X.-J. Huang, C.-C. Wei, Y.-L. Wu, W.-H. Zhang, and Y.-F. Zhou, Antiprotons from dark matter annihilation through light mediators and a possible excess in AMS-02 pbar/p data, Phys. Rev. D **95,** 063021 (2017).

[63] S.-J. Lin, X.-J. Bi, J. Feng, P.-F. Yin, and Z.-H. Yu, Systematic study on the cosmic ray antiproton flux, Phys. Rev. D **96,** 123010 (2017).

[64] M. Aguilar, L. Ali Cavasonza, G. Ambrosi et al., Precision Measurement of the Boron to Carbon Flux Ratio in Cosmic Rays from 1.9 GV to 2.6 TV with the Alpha Magnetic Spectrometer on the International Space Station, Phys. Rev. Lett. **117,** 231102 (2016).

[65] M. Aguilar, L. Ali Cavasonza, G. Ambrosi et al., The Alpha Magnetic Spectrometer (AMS) on the international space station: Part II - Results from the first seven years, Phys. Rep. **894,** 1 (2021).

[66] D. Kerszberg, M. Kraus, D. Kolitzus et al. (H.E.S.S. Collaboration), The cosmic ray electron spectrum measured with H.E.S.S., in Proceeding of 35th ICRC (2017), https://www.mpi-hd.mpg.de/hfm/HESS/pages/home/som/2017/09/.

[67] G. Ambrosi, Q. An et al. (DAMPE Collaboration), Direct detection of a break in the teraelectronvolt cosmic-ray spectrum of electrons and positrons, Nature (London) **552,** 63 (2017).

[68] M. Aguilar, L. Ali Cavasonza, B. Alpat et al., Towards Understanding the Origin of Cosmic-Ray Electrons, Phys. Rev. Lett. **122,** 101101 (2019).

[69] M. Aguilar, L. Ali Cavasonza, G. Ambrosi et al., Towards Understanding the Origin of Cosmic-Ray Positrons, Phys. Rev. Lett. **122,** 041102 (2019).